**Egyptian Journal of Chemistry**

**http://ejchem.journals.ekb.eg/**

# Preparation of Non-stoichiometric Zinc Ferrite/Magnetite [$(Zn_xFe_{1-x})O.Fe_2O_3$] Nanoparticles: Adsorption and Biological Activity

**Amal M. Ibrahim,*[a] Fatma A. Ibrahim,[b,c] Mohamed M. Selim[a]**

[a]*Physical Chemistry Department., National Research Centre, NRC, Egypt.*
[b]*Department of Chemistry, Faculty of Science, King Khalid University, Abha, Saudi 42 Arabia.*
[c]*Physical Chemistry Department, Faculty of Women for Art, Science and Education, 44 Ain Shams University, Cairo, Egypt*

**Abstract**

Magnetic nanomaterials especially ferrites are gaining more interest recent years for environmental and biomedical applications. The preparation of non-stoichiometric zinc ferrite nanoparticles [$(ZnxFe_{1-x})O•Fe_2O_3$] was achieved by a modified co-precipitation route. The obtained samples were characterized by Scanning electron microscopy (SEM), X-ray diffraction (XRD), and Vibrating Sample Magnetometer (VSM). All samples have crystallite sizes in the range of 3-7 nm. The hysteresis curves for magnetic properties showed a very low coercivity tending to zero for pure $ZnFe_2O_4$.This behavior is attributed to the crystallite size which is smaller than that of a single domain. The prepared samples were evaluated upon removal of Alizarin yellow dye and various parameters for the adsorption process were studied. The adsorption process showed high removal efficiency, which reached to 93% in the case of the zinc ferrite sample with maximum zinc molar ratio. The removal efficiency was found to increase with increasing molar ratio of Zn. The obtained nanopowders were also tested for their antimicrobial activity against Gram-negative bacteria, Gram-positive bacteria, and pathogenic yeast. The sample with the highest molar ratio of zinc showed potent antimicrobial activity against Bacillus cereus, Staphylococcus aureus, and Candida albicans. The $ZnFe_2O_4$ sample is considered a promising antimicrobial agent.

***Keywords***: magnetic nanomaterials; Zinc ferrite; magnetic properties; antimicrobial activity.

## 1. Introduction

In recent decades, the water crisis is taking more effort and research to improve water treatment techniques to reuse industrial wastewater and many effluents of polluted water. One of the problems that arise after treatment of wastewater is the removal of the treatment agents from the water effluent to be able to reuse it. The manipulation of magnetic materials to act as wastewater treatment agents either as adsorbents for organic and inorganic pollutants or as disinfection agents for removing pathogenic microorganisms, this manipulation is considered a solution for the removal problem of the adsorbents. It is easy to remove magnetic agents after the wastewater treatment simply by applying an external magnetic field. Iron-based magnetic nanoparticles have attracted increasing attention due to their wide applications. Among iron-based magnetic materials, ferrites, a ferromagnetic metal oxide, are widely used in many fields, including drug delivery systems and pharmaceuticals [1,2], cancer treatment [3,4], sensors and biosensors [5-7], microwave absorbing materials, and magnetic resonance imaging [8,9]. Ferrites have been classified into three classes based on their crystal structure, hexagonal ferrites (hexaferrite), garnet, and spinel ferrites. Hexaferrites (Figure-1-a) have the general formula ($MFe_{12}O_{19}$) obtained by stacking two different types of structural blocks. Hexaferrites have the advantage of having a layer of oxygen atoms in a closed-backed structure [10, 11].

*Corresponding author, e-mail: amozarei@gmail.com (Amal M. Ibrahim)
**Receive Date:** 22 April 2022, **Revise Date:** 28 June 2022, **Accept Date:** 17 July 2022, **First Publish Date:** 17 July 2022
DOI: 10.21608/EJCHEM.2022.135033.5953
©2022 National Information and Documentation Center (NIDOC)

Garnet metal ferrites have the general formula ($MFe_5O_{12}$) (Figure-1-b). In garnet ferrite, all octahedral and tetrahedral sites occupy by metallic cations [12]. Iron-based spinel ferrites have a face-centered cubic structure (Figure-1-c). Spinel ferrites have the formula $[\boldsymbol{M}_{1-x}^{+2}\boldsymbol{Fe}_{x}^{+2}]_A[\boldsymbol{M}_{x}^{+2}\boldsymbol{Fe}_{2-x}^{+3}]_B$. Where (A) represents the tetrahedral sites, (B) represents the octahedral sites, and (x) represents the trivalent iron ions in the tetrahedral positions [13].

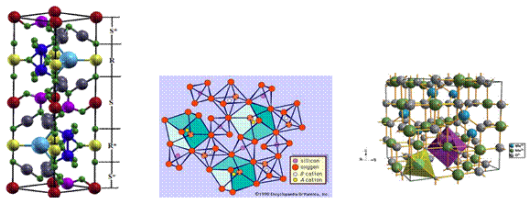

**(a)** **(b)** **(c)**

Figure -1-**a**-hexaferrite crystal structure [14], **-b-** Garnet metal ferrite [15], and **-c-** spinel ferrite crystal structure [16]

Zinc ferrite is one of the most interesting spinel metal ferrites. Nanostructured zinc ferrite exhibits exceptional physical, chemical, and magnetic properties. Zinc ferrite has the formula $ZnFe_2O_4$, in which divalent zinc ions occupy the tetrahedral sites. $ZnFe_2O_4$ represents a breakthrough in gas sensing applications [14], magnetic fluid hyperthermia in cancer treatment [4, 17], and as an MRI contrast agent [18]. Ferrites have also attracted attention in water treatment as photocatalysts and adsorbents by themselves or in combination with other materials in the form of composites [19-21]. Ferrites exhibit antimicrobial activity and are therefore being investigated for many biomedical applications [22-24]. Zinc ferrite nanoparticles have been synthesized by various techniques [25], including solid-state reaction [26], sol-gel technique [27], hydrothermal synthesis [28], ball milling [29], microwave-assisted technique [30], and co-precipitation technique [31, 32]. The co-precipitation technique is considered the most studied technique for $ZnFe_2O_4$ nanoparticles (ZFNps) preparation. Co-precipitation allows the doping content, the purity, and crystallite size of the produced nanoparticles to be precisely controlled [33]. In previous publications, ferrites were prepared by coprecipitation using a neutralizing agent, but the product needs further heat treatment. The ferrites obtained in these cases have non-uniform crystallite size due to the heat treatment [34-36]. In this work, ZFNps with different stoichiometric zinc molar ratios were prepared by the co-precipitation technique with slight modifications to increase homogeneity without the need for further heat treatment. The prepared ferrite nanoparticles (ZFNps) were characterized by X-ray diffraction (XRD), scanning electron microscopy (SEM), and vibrating sample magnetometer (VSM). In addition, the biological activity of ZFNps against Gram-negative bacteria, Gram-positive bacteria, and pathogenic yeasts was investigated. The obtained ZFNps were evaluated in the removal of organic dye (Alizarin Yellow R) from aqueous solutions using batch adsorption experiments, where different adsorption parameters were investigated.

## 2. **Experimental**

### *2.1. Materials*

Ammonium hydroxide solution ($NH_4OH$) 30%, ferric chloride ($FeCl_3.H_2O$) and ferrous sulphate ($FeSO_4.7H_2O$) were supplied by Adwic Company - Egypt. Zinc chloride ($ZnCl_2$) was supplied by Aldrich Company. All chemicals and materials were used as received. Alizarin Yellow R ($C_{13}H_9N_3O_5$, molecular weight: 287.23 g/mol) was supplied by Sigma-Aldrich in 99% purity (Figure-2-).

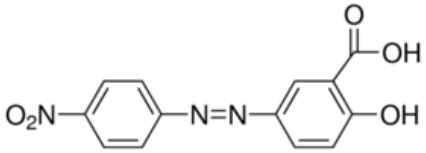


Figure -2- Alizarin Yellow R

### *2.2. Preparation of Different ZFNps with Different Molar Ratios of Zinc*

Zinc ferrite nanoparticles (ZFNps) were prepared by coprecipitation from the solution of precursors $FeSO_4.7H_2O$ (ferrous sulphateheptahydrate), $FeCl_3.6H_2O$ (ferric chloride hexahydrate), and $ZnCl_2$ (zinc chloride) in different molar ratios of $Zn^{2+}$, so that the ZFNps are represented as $(ZnxFe_{1-x})O.Fe_2O_3$ in which the divalent zinc replacing the divalent iron ions. The coprecipitation process was carried out by dropwise addition of ammonium hydroxide solution with constant agitation to achieve the pH of the reaction mixture pH = 10 at 50°C. The obtained ZFNps samples are designated as ZFNps (0), ZFNps (1), ZFNps (2), ZFNps (3) and ZFNps (4) and correspond to $Fe_3O_4$,$(Zn_{0.25}Fe_{0.75})O.Fe_2O_3$, $(Zn_{0.5}Fe_{0.5})O.Fe_2O_3$, $(Zn_{0.75}Fe_{0.25})O.Fe_2O_3$and $ZnFe_2O_4$, respectively.

### *2.3. Biological Activity Study:*

Qualitative evaluations were performed on nutrient agar plates according to Mostafa et al., 2016 [37]. Inoculation of all microorganisms was prepared from fresh broth cultures incubated overnight at 37°C [38]. The spore suspension of the pathogenic strains was prepared and adjusted to approximately 0.5 McFarland standard (1.5 × 108 /ml). 25.0 µL of the bacterial and yeast suspensions were inoculated into each plate with 20.0 mL of sterile nutrient agar medium (NA). After the medium had cooled and solidified, 100 µL of the prepared samples were applied to the wells (well diameter = 0.9 mm) - previously prepared- on the incubated agar plates. These colonized plates were placed in the refrigerator for one hour and then incubated at 37 ºC for 24 hours. The inhibition zones (ZI) were measured in mm [37]

### *2.4. Characterization Techniques*

X-ray diffraction analysis was performed using an X-ray diffractometer (Shimadzu 7000, USA) to evaluate the phase composition. XRD spectra were obtained using a 30 kW rotating anode diffractometer with a copper target. XRD spectra were acquired between 20◦ and 80◦ (2) in a continuous scan at 4◦/min using standard 2 geometry. The morphology of the synthesized powders was studied by field emission scanning electron microscope (FESEM) using Quanta FEG250 instrument. The magnetic properties were investigated using Vibrating Sample Magnetometer (VSM) Lake Shore Model 7410 (USA) with general features: moment measurement range 0.1 x $10^{-6}$ emu to 1000 emu. Time constants (TC) (0.1, 0.3, 1.0, 3.0, or 10.0 seconds), output stability better than ±0.05% of full scale per day with fixed coil geometry and constant field and temperature.Absolute accuracy is better than 1% of reading ±0.2% of full scale (when DUT and calibrant are geometrically identical). Repeatability is better than ±1%, or ±0.15% of full scale, whichever is greater, fixed angle of rotation, field accuracy in Gauss 1% of reading or ±0.05% of full scale.

### *2.5. Adsorption Study:*

The prepared ZFNps were tested for adsorption Alizarin Yellow R dye from its aqueous solutions at room temperature using the the patch experiment technique. The dye solutions were prepared by adding the appropriate weight in distilled water to obtain the desired concentration. The experiments were performed using thermal shaker devices. Different variables controlling the adsorption process were studied: contact time intervals (15-150 minutes), ZFNps dose varied from 1g/L to 4g/L, and initial dye concentrations (25, 50, 75, 100 mg/L). The dye concentrations were monitored during the adsorption process using a UV-vis spectrophotometer. The percent removal of the dye was calculated using equation (1).

$$\%\ \boldsymbol{Removal} = \frac{\boldsymbol{C_o - C}}{\boldsymbol{C_o}} \times \mathbf{100} \qquad \boldsymbol{equation}\ (\mathbf{1})$$

Where$C_o$, is the initial dye concentration mg/L, and $C$ is the dye concentration after adsorbent separation at the end of the conducted experiment.

The removal efficiency was calculated as the amount of dye (mg) adsorbed per amount of ZFNps (g) using equation (2).

$$\boldsymbol{Q\left(mg/g\right)} = \frac{\boldsymbol{V\ (C_o - C)}}{\boldsymbol{M}} \qquad \boldsymbol{equatin}\ (\mathbf{2})$$

Where Q is the removal efficiency, V is the volume of the solution (mL), and M is the mass of solid adsorbent (g).

## *3. Results and Discussion*

The X-ray diffraction patterns of the prepared ZFNps with different Zn molar ratios are shown in (Figure-3-). The molar stoichiometry of the zinc ions replacing the iron ions in $Fe_3O_4$ to be zero, 0.25, 0.5, 0.75, and 1.0. The sample ZFNps (0) representing pure $Fe_3O_4$ showed a significant pattern for magnetite in agreement with the JCPDS card no. (79-0417). The characteristic peaks for $Fe_3O_4$ were located at 2θ = 30.66, 36.07, and 62.8º. In the samples labeled ZFNps (1) and ZFNps (2), which have compositions of $(Zn_{0.25}Fe_{0.75})O\text{-}Fe_2O_3$ and $(Zn_{0.5}Fe_{0.5})O\text{-}Fe_2O_3$, respectively, divalent zinc ions were introduced into the spinel structure instead of iron ions. The intensity of the peaks corresponding to magnetite was decreased. On the other hand, no significant peaks were detected for the ferrite phase, which could be due to the amorphous nature of the sample as well as the low molar ratio of zinc ferrite formed in the products. For the sample designated ZFNps (3) with composition $(Zn_{0.75}Fe_{0.25})O\text{-}Fe_2O_3$, the significant peaks for zinc ferrite were found at 2θ = 32.56, 41.1, 44.7, and 48.9º in agreement with JCPDS card no. (36-0398). The occurrence of the ferrite pattern was

accompanied by a significant pattern of magnetite. For the sample labeled ZFNps (4), which represents $ZnFe_2O_4$ as pure ferrite, the XRD pattern showed only peaks of spinel zinc ferrite crystal structure. All sample patterns showed a broadening of the peaks of the phases obtained, indicating low crystallinity. The crystallite size of both the ferrite and magnetite phases was calculated using Scherer's equation (3) and were in the range of 3-7nm.

$$L = \frac{0.089\,\lambda}{\beta \cos\theta} \qquad \text{equation (3)}$$

Where β is the FWHM of diffraction peak, λ is the wavelength of X-ray (0.154 nm), L is the crystallite size, and θ is the Bragg peak position.

Scanning electron micrographs were shown in (Figure-4-) for different ZFNps samples. The SEM images were accompanied by the EDEX analysis data(Figure-5-). The images show a strong agglomeration of the powder obtained from the nanoparticles. The image for the sample ZFNps (0) showed a homogeneous agglomeration of the nanoparticles of $Fe_3O_4$. For samples ZFNps (1), ZFNps (2), and ZFNps (3), the images show some degree of heterogeneity, as both $Fe_3O_4$ and $ZnFe_2O_4$ were represented. In the case of sample ZFNps (4), representing the zinc ferrite phase $ZnFe_2O_4$. Zinc ferrite appeared as aggregates of spherical nanoparticles. The EDEX analysis data for the samples are in agreement with the theoretical atomic percentages for all components

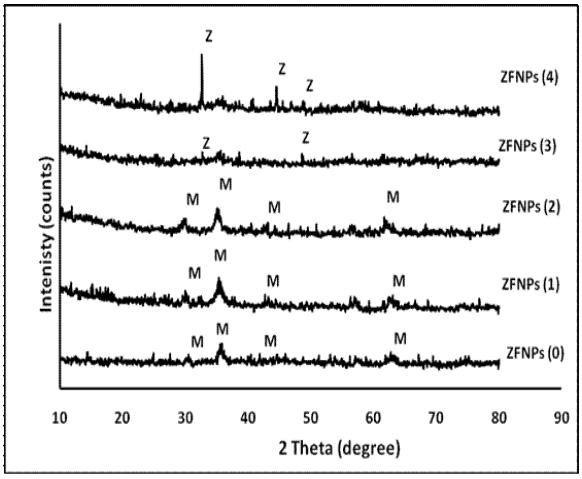


Figure -3- XRD diffractograms for the prepared samples with different compositions, the peaks corresponding to the magnetite phase denoted as M and that for zinc ferrite phase denoted Z.

The magnetic properties of the obtained samples were studied by establishing the relationship between the magnetization (M) and the applied magnetic field strength (H). The curves of the hysteresis loop obtained in (Figure-6-) show hysteresis loop curves of zero coercivity in all hysteresis loops. The sample which is labelled ZFNps (4) - representing the pure zinc ferrite $ZnFe_2O_4$ - shows a linear magnetization curve indicating superparamagnetic properties of zinc ferrite with single domain character [39,40]. The saturation magnetization (Ms) decreased with the increase of the molar ratio of zinc ferrite in the composition of the prepared ZFNps (Figure-7-) with Ms being the lowest for the pure zinc ferrite sample. The decrease of "Ms" with the introduction and increase of $Zn^{2+}$ ions in the spinel crystal structure could be due to the decrease in the ability of $Fe^{3+}$ ions to be interchangeable between the tetrahedral and octahedral sites [41]. In the obtained samples, the calculated crystallite size range is much smaller than the critical size for both $Fe_3O_4$ and $ZnFe_2O_4$, and the crystallite size decreases slightly with the increase of the molar ratio of zinc. This could be a reason why does "Ms" decrease with increasing zinc ferrite formation in the products.

### *4. The Biological Activity of The Obtained ZFNps*

Zinc ferrite is reported as a biologically active material and getting more attention during past decades in many biological applications [42]. ZFNps samples were tested for inhibition of Gram-negative bacteria [Escherichia coli (ATCC25922) and Pseudomonas aeruginosa (ATCC27853)], Gram-positive bacteria [Bacillus cereus (ATCC 6629) and Staphylococcus aureus (ATCC 6538)], and pathogenic yeasts (Candida albicans (ATCC 10231)). The inhibition zones value are shown in Table (1) as the diameter of the zone of inhibition in millimeters of the sample.

All samples showed no inhibition effect for Escherichia coli and Pseudomonas aeruginosa. These results could be explained by the inability of the prepared samples to have the effect required for the destruction of this bacterial species. The mode of action in inhibiting Gram-negative bacteria depends on the destruction or injury of the bacteria cell wall to penetrate it and affect bacterial metabolism. The ZFNps(3) and ZFNps(4) samples showed excellent

inhibitory activity against both Gram-positive bacteria and pathogenic yeasts, exhibiting broad-spectrum antimicrobial activity against both bacteria and fungi. These two samples can affect the cell wall of Gram-positive bacteria by binding with it and causing inhibition of nucleic acid synthesis, which in turn affects metabolic activity in bacterial cells [43]. The samples designated ZFNps(0)&(1) showed low antifungal activity against pathogenic yeast (Candida albicans). Meanwhile, samples ZFNps(2), ZFNps(3), and ZFNps(4) showed high antifungal activity, which could be explained by the disruption of the fungal cell wall structure [44]. Sample ZFNps(4) showed excellent antimicrobial activity against both Gramme-positive bacteria (Bacillus cereus & Staphylococcus aureus) and pathogenic yeast (Candida albicans). The inhibition zone of 20-28 mm, outperforms the other two samples ZFNps (2 & 3), which have inhibition zones of 11-26 mm and 20 mm, so the sample with the code ZFNps (4) can be considered a promising antimicrobial agent.

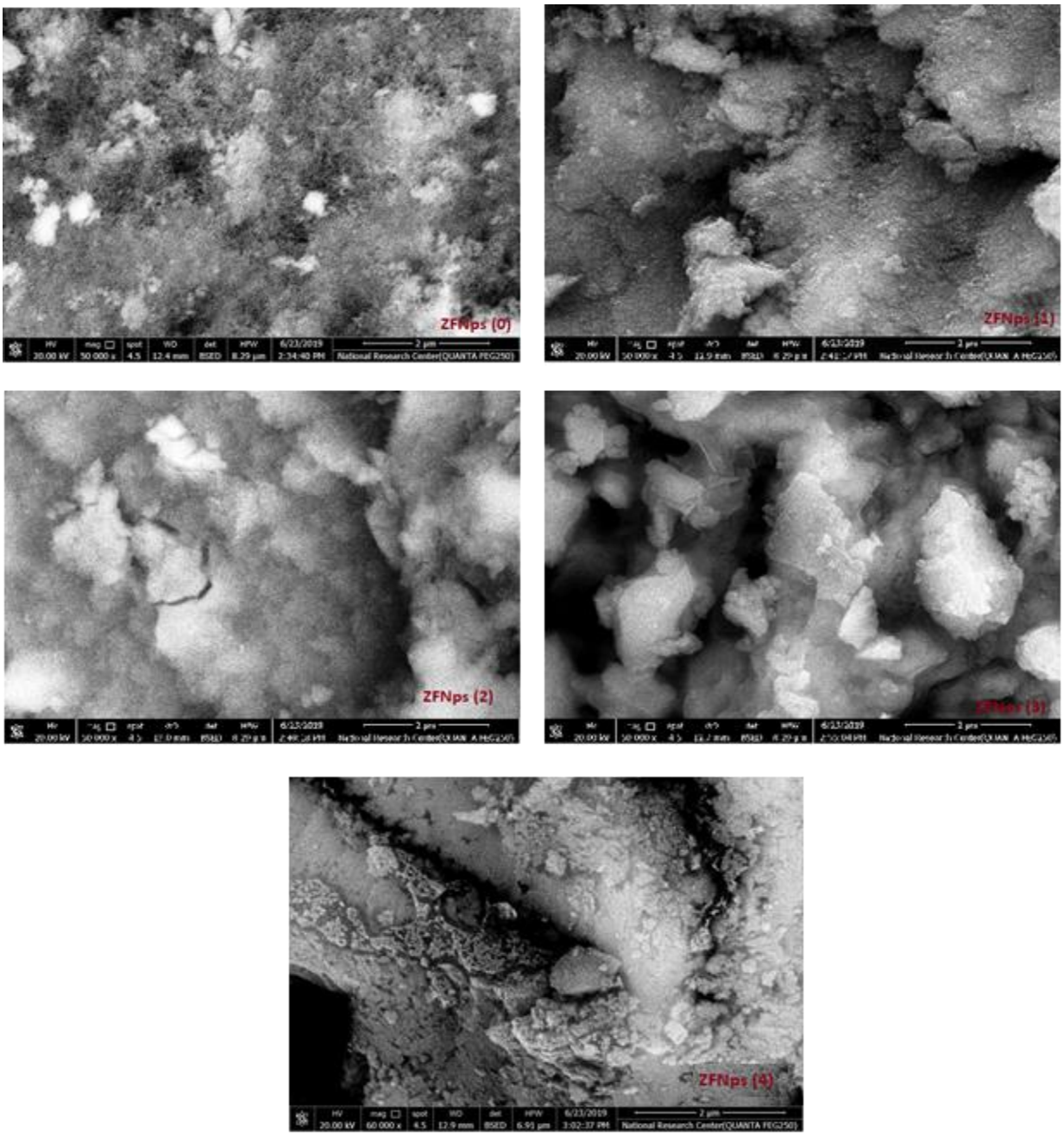


Figure -4- Scanning Electron Microscope Images for prepared samples

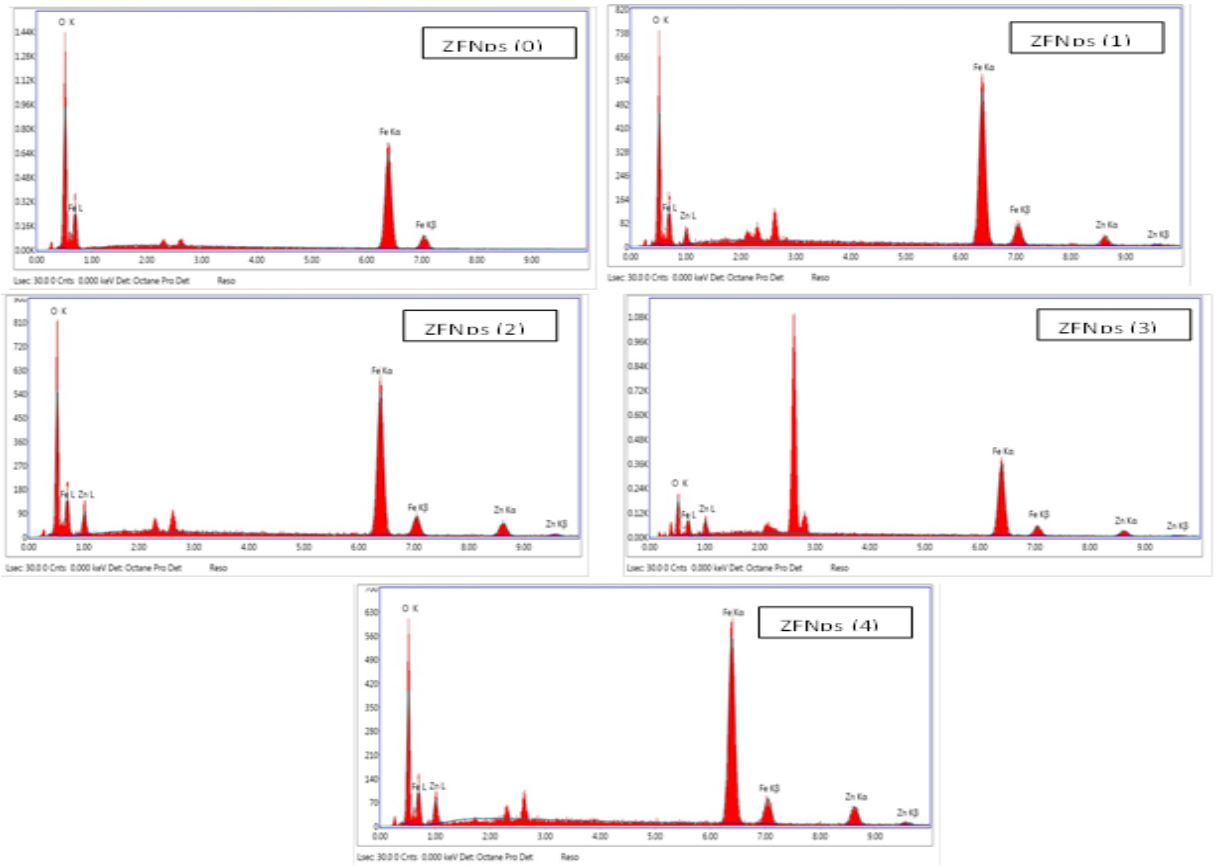


Figure -5- EDEX analysis data for prepared samples

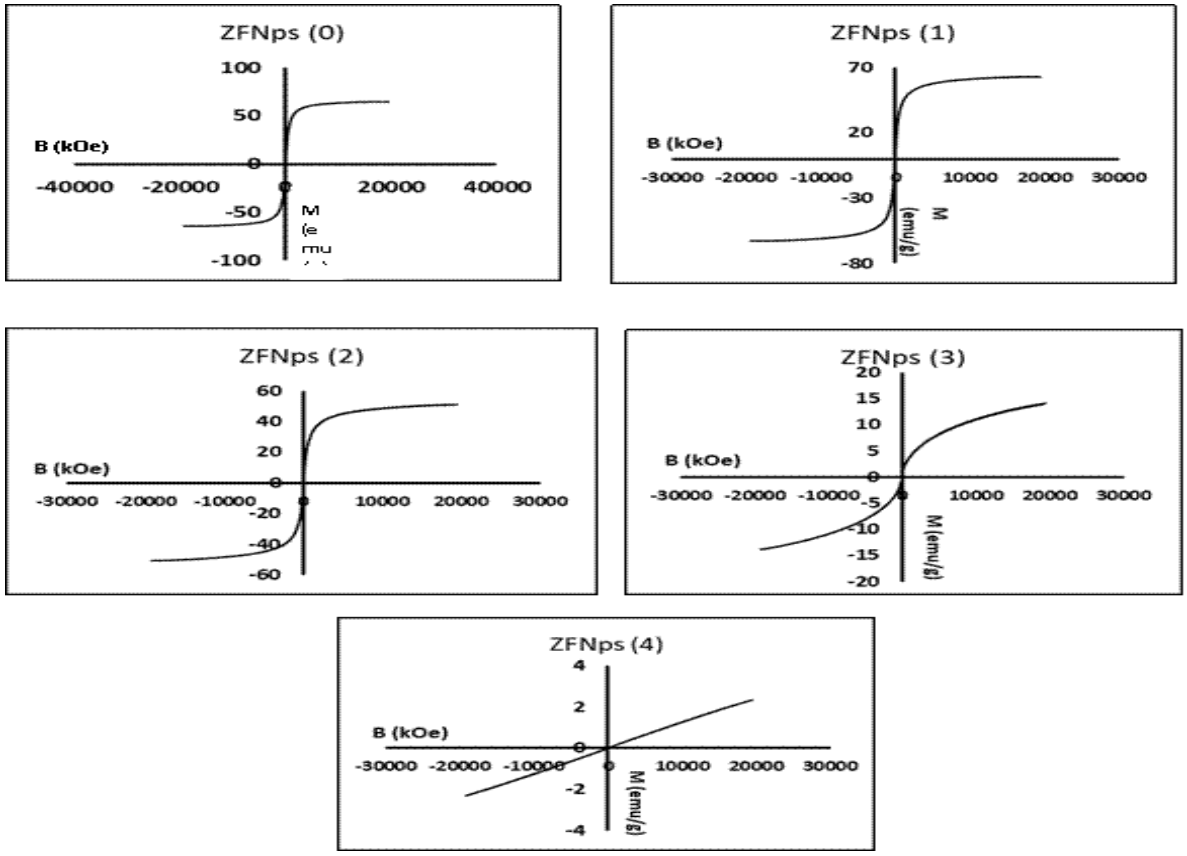


Figure -6- magnetic hysteresis loops of the prepared $(Zn_xFe_{1-x})O.Fe_2O_3$ samples

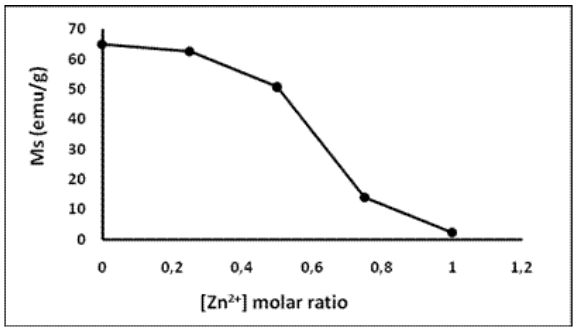


Figure -7- the saturation values obtained from magnetization magnetometer measurements for the prepared samples as a function in $Zn^{2+}$ molar ratio

**Table (1): Inhibition zone diameter (millimeter) of the samples**

| Samples Test bacteria | ZFN ps(0) | ZFN ps(1) | ZFN ps(2) | ZFN ps(3) | ZFN ps(4) |
|---|---|---|---|---|---|
| *Escherichia coli* | ** | ** | ** | ** | ** |
| *Pseudomonas aeruginosa* | ** | ** | ** | ** | ** |
| *Bacillus cereus* | ** | ** | ** | 17.0 | 23.0 |
| *Staphylloco cusaureus* | ** | ** | ** | 11.0 | 20.0 |
| *Candida albicans* | ** | ** | 20.0 | 26.0 | 28.0 |

### *5. Sorption efficiency of the ZFNps on removal of Alizarin yellow R*

Some factors controlling the sorption process of the dye on the prepared ZFNps with different molar compositions were investigated.

### *5.1. Effect of Contact Time of Adsorption Experiment:*

The effect of the contact time of the sorption process is first studied to determine the equilibrium time at which the sorption process reaches dynamic equilibrium and appears to remain constant. The effect of contact time is studied on different ZFNps for 50 ppm dye at room temperature (20°C) and stirring speed of 200 rpm. (Figure -8-) shows that the removal efficiency increases dramatically in the first few minutes, and the rate of increase becomes very slow until equilibrium. At the equilibrium the amount of adsorbed dye equals the amount of desorbed dye, and no further increase is observed. At this point, adsorption represents the maximum capacity under these conditions [45]. In this study, an equilibrium time of 90 minutes was determined. It can be seen from the figure that the removal efficiency is lowest for the ZFNps(0) sample which is magnetite ($Fe_3O_4$) without zinc addition. Then the removal efficiency starts to increase with the increasing molar ratio of zinc and reaches its maximum with ZFNps(4), which is pure zinc ferrite $ZnFe_2O_4$.

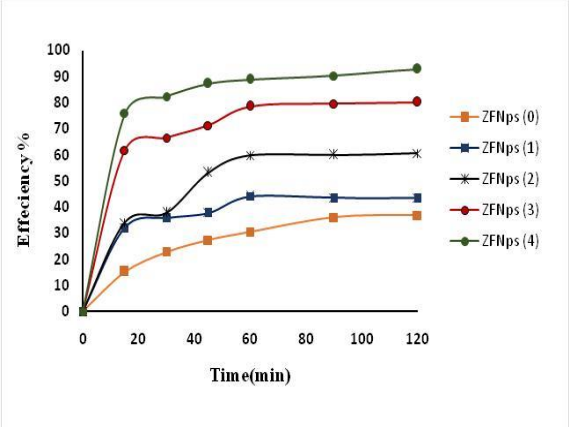


Figure -8- effect of contact time on adsorption of Alizarin yellow dye on different ZFNPs at 20°C and 200 rpm

### *5.2. Effect of Adsorbent Dosage*

The effect of the amount of different ZFNps adsorbents was shown in (Figure -9-). It can be observed that the removal efficiency increases with the increasing amount of adsorbent. Also, the removal efficiency of different non-stiometric ZFNps showed that as the molar ratio of zinc increases, the efficiency increases and reaches maximum efficiency in the case of sample ZFNps (4), which is a pure zinc ferrite sample $ZnFe_2O_4$.

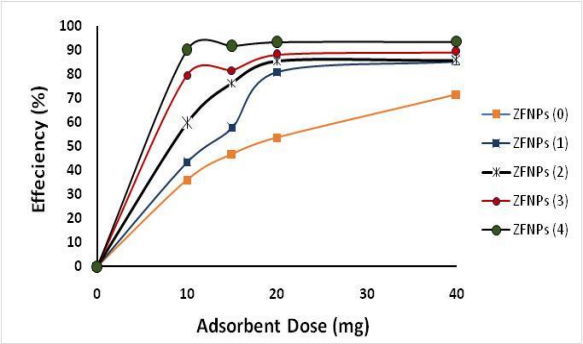


Figure -9- effect of ZFNPs dose on different ZFNPs at 20°C and 200 rpm

### *5.3. Effect of Initial Dye Concentration*

The effect of the different initial dye concentrations on the different molar compositions of

nonstiometric zinc ferrite nanoparticles was studied using the optimum adsorbent dose and contact time (15 mg & 90 minutes) as shown in (Figure -10-). The percentage removal of dye decreased with the increase of initial dye concentration from 25 to 100 mg/L. This behavior could be due to the fact that at a low dye concentration, any single adsorbate ion present in the solution can easily reach the active site of the adsorbent, and consequently high adsorption activity was observed. On the other hand, at higher dye concentrations, the adsorbed ions have difficulty in reaching the active site of the adsorbent, and the saturation of the active sites of the adsorbent prevents further uptake of the dye, resulting in a decreasing behavior. The adsorption efficiency increases with increasing molar ratio of zinc and reaches its maximum in the pure zinc ferrite sample ZFNps(4).

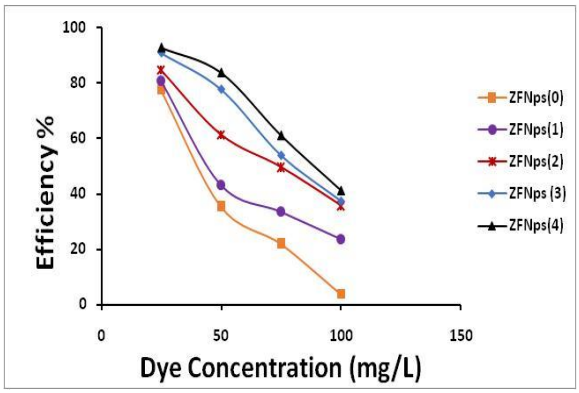


Figure -10- effect of dye concentration on adsorption of Alizarin yellow dye on different ZFNPs at 20ºC and 200 rpm

### *5.4. Effect of pH*

The effect of pH is one of the most important parameters that affect the adsorption processes, effect of pH on adsorption of Alizarin yellow R dye on different prepared zinc ferrite nanoparticles is studied on pH range from 2 to 10 (Figure-11-). The relationship revealed that the adsorption efficiency decreases with increasing pH, also the efficiency increases as the molar ratio of zinc increases. The efficiency of zinc ferrite increases in the acidic medium and decreases in the basic medium, this behavior is devoted to the interaction between charges on both dye molecules and ZFPps. Alizarin yellow R dye has two hydroxyl groups that undergo protonation/deprotonation upon acidic/basic medium change, it also contains an azo group which is transformed into quinone group in basic medium and vice versa Scheme I [46]. So, alizarin yellow is acquiring a negative charge in the basic medium and a positive charge or less negative in the acidic medium. On the other hand, zinc ferrite is reported to have a pH zero point at 9.3, this means that ZFNps acquire a positive charge in acidic and neutral media meanwhile acquiring a negative charge in the basic medium [47]. This is not the only factor related to the ferrite structure, zinc ferrite could be considered an amphoteric material in which iron oxide sites undergo protonation and deprotonation exchange with pH change Scheme II.[48]. These all factors explain the high adsorption efficiency in the acidic medium due to electrostatic attraction between dye molecules and adsorbent molecules (ZFNps), and low efficiency in the basic medium due to repulsion between them.

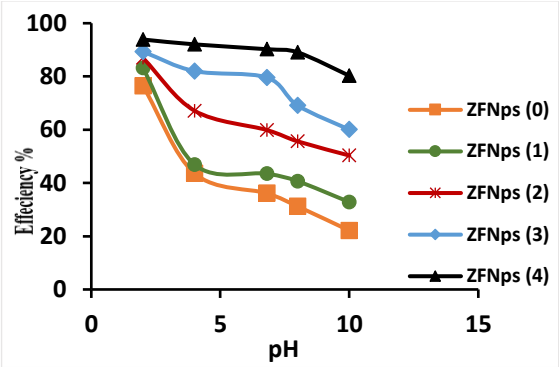


Figure -11- effect of pH on adsorption of Alizarin yellow dye on different ZFNPs at 20ºC and 200 rpm

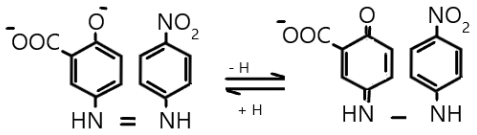

**Scheme I: Alizarin yellow R dye transformation**

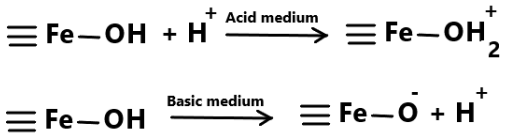

**Scheme II: Iron oxide sites transformation**

### *5.5. Sorption kinetics modeling*

the adsorption process of Alizarin Yellow R dye onto nonstiometric zinc ferrite nanoparticles was investigated using the fitting of the kinetic data obtained in three different kinetic models which are pseudo-first-order reaction rate, pseudo-second-order reaction rate, and intraparticle diffusion models.

Lagergren and Svenska expression (equation 4) is used to elucidate the pseudo-first-order reaction model. Lagergren constant was calculated to see if

the adsorption process obeys the pseudo-first-order reaction model or not [49].

$$\ln(q_e - q) = \ln q_e - k_1 t \qquad equation\ (4)$$

Where $q_e$ and q are the amounts of dye adsorbed (mg/g) at equilibrium and at time t (min), respectively, and $k_1$ is the rate constant of adsorption (L/min). The values of $k_1$, $q_e$ calculated from the equation and the correlation coefficient ($R^2$) values of fitting the first-order rate model at different concentrations are presented in table 2. The linear relationship between ln ($q_e$–q) versus time is represented in (figure -12-), the $R^2$ values are too low indicating that the process of Alizarin Yellow R dye adsorption did not obey the first-order rate kinetics. Also, the theoretical values of $q_e$ calculated from the straight line equation is different than that the experimentally determined, which insure that the removal process didn't fit with pseudo-first-order reaction model.

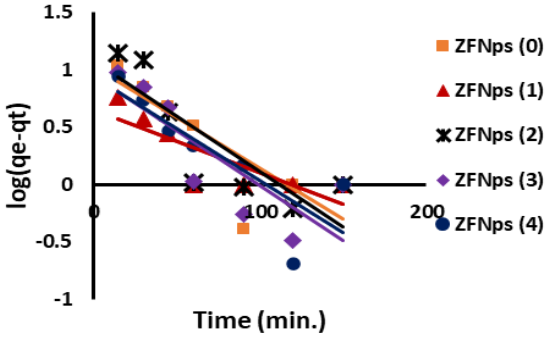


Figure -12- Pseudo-first-order plots for different nonstiometric zinc ferrite nanoparticles (at 20°C, 200 rpm).

The pseudo-second-order model expressed by Ho and McKay's in which adsorption data were studied using equation (5)

$$t/q_t = \left(1/K_2 q_e^2\right) + t/q_e \qquad equation\ (5)$$

Where $k_2$ is the equilibrium rate constant of the pseudo-second order (g/mg min). The linear relationship between t/qt versus t (min.) are shown in (Figure –13-). The $k_2$, $q_e$ and correlation coefficients ($R^2$) were calculated from this plot and are given in Table 2. The correlation coefficient ($R^2$) values are high enough to prove that the adsorption process of Alizarin Yellow R dye is obeying the pseudo-second order model. Also, the calculated values of $q_e$ is close to the values determined experimentally, which support the same conclusion [50, 51]. This behavior confirms that the sorption process for Alizarin yellow R dye using different nonstiometric zinc ferrite nanoparticles is depending mainly on chemisorption process.

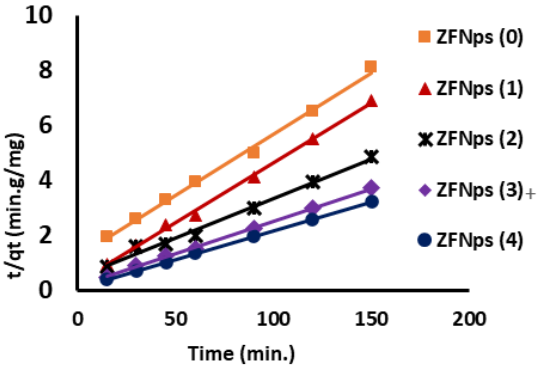


Figure -13- pseudo-second- order plots for different nonstiometric zinc ferrite nanoparticles (at 20°C, 200 rpm).

Weber–Morris established the intraparticle diffusion model by correlation the adsorption uptake with $t^{1/2}$ Eq. (6)

$$q_t = k_d t^{1/2} + c \qquad equation\ (6)$$

Where, $k_d$ is the intra-particle diffusion rate constant. Values of C are related to the thickness of the boundary layer. The relationship for studying intraparticle diffusion is represented in (figure -14-). In case of the relation between $q_t$ versus $t^{1/2}$ will be linear this, indicates that intraparticle diffusion occurs, and if the plot passes through the origin, then the rate determining step in adsorption process is only due to the intraparticle diffusion [52].

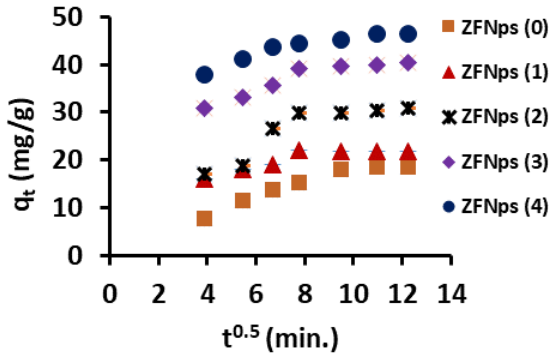


Figure -14- intraparticle diffusion plots for different nonstiometric zinc ferrite nanoparticles (at 20°C, 200 rpm).

Intraparticle diffusion plot is consisted from two regions, the first region belonged to surface adsorption in which film formation occurs. Meanwhile the second region in the plot represents the adsorption process in which the intraparticle diffusion is the limiting step. The non-linearity of the plot even it is close to linear nature indicates that

intraparticle diffusion occurs but the fact that the second region of the plot (plateau region) is not passing through the origin point indicating that the intraparticle diffusion is not the only determining step in adsorption process.

### *5.6. Adsorption Mechanism*

The aqueous solution of Alizarin yellow dye has pH = 6.8, which is almost neutral and slightly acidic. At this pH, dye molecules acquire a positive charge (as mentioned earlier). Meanwhile, ZFNps acquire a negative charge because the solution pH is less than pH zero. The opposite charges on the adsorbate and adsorbent lead to electrostatic attraction. This attraction initiates and facilitates the diffusion of the adsorbate toward the adsorbent surface. Once dye molecules get closer to ZFNps the oxygen atoms in the spinel structure sites act as active adsorption sites due to their negative partial charge due to the electron cloud. Hydrogen-bonding could be formed in this case, increasing the strength of adsorbate–adsorbent interaction. As the molar ratio of zinc atoms increases in the spinel structure, the efficiency of the adsorption increases. This could be devoted to the fact that the insertion of zinc atoms replacing the iron atoms could cause defect sites which increase the number of the active site and subsequently enhance the adsorption efficiency.

### *Conclusions*

- Magnetic nanoparticles are becoming increasingly important for environmental and biomedical applications. Treatment of wastewater involves both remediations of organic and inorganic pollutants and disinfection of pathogenic microbes. It is a goal to achieve both processes with the same treatment agent**.**
- Non-stoichiometric zinc ferrite nanoparticles were successfully prepared. The obtained samples showed a tendency to superparamagnetic materials with the increase of $Zn^{2+}$ molar ratio up to pure $ZnFe_2O_4$, which exhibits superparamagnetic nature. Normal ferrites show ferromagnetic behavior, but when the crystallite size was smaller than the single domain size, the nanoparticles show superparamagnetic properties.
- All prepared samples have crystallite size (3-7nm) smaller than a single domain, which leads to hysteresis loops with zero coercivity. The hysteresis curve of $ZnFe_2O_4$ shows a superparamagnetic material without saturation magnetization (Ms).
- These magnetic properties facilitate the separation of adsorbing nanoparticles after treatment by applying a magnetic field, which is the main goal of such a study of magnetic materials.
- Moreover, the obtained ZFNPs were studied in the removal of the dye Alizarin Yellow R from its aqueous solutions; the efficiency of ZFNPs reaches 93% in room temperature and normal pH of the dye solution
- The biological activity of the prepared samples was studied as inhibitors for gramme-negative, gramme-positive and pathogenic yeasts. The biological studies showed a high efficiency of $ZnFe_2O_4$ as an antimicrobial agent against gramme-positive bacteria and pathogenic yeasts.
- The increase in $Zn^{2+}$ molar ratio has a positive effect on all the applications studied; this could be due to the replacement of $Zn^{2+}$ ions with a smaller atomic size than $Fe^{2+}$ in the tetrahedral sites in the spinel crystal structure.
- $ZnFe_2O_4$ nanoparticles are considered excellent candidates for the removal of organic dyes and pathogenic microbes.
- The sorption process for Alizarin yellow R dye using different nonstiometric zinc ferrite nanoparticles is best fitted with the pseudo-second- order model which indicates that the adsorption process is mainly a chemisorption process.

Table 2: The pseudo first-order and second-order kinetic parameters for Alizarin yellow R dye removal using different nonstiometric zinc ferrite nanoparticles

| **Kinetics model** | $q_{exp}$ **mg/g** | **Pseudo-first-order** | | | **Pseudo-second- order** | | |
|---|---|---|---|---|---|---|---|
| **Sample** | | $K_1$ $min.^{-1}$ | $q_e$ mg/g | $R^2$ | $K_2$ | $q_e$ | $R^2$ |
| **ZNFPs(0)** | 18.506 | 0.0088 | 2.786 | 0.6923 | 0.00234 | 22.522 | 0.9958 |
| **ZNFPs(1)** | 21.724 | 0.0055 | 1.928 | 0.6880 | 0.00742 | 22.8833 | 0.9977 |
| **ZNFPs(2)** | 30.896 | 0.0096 | 2.934 | 0.7028 | 0.00224 | 34.7222 | 0.9906 |
| **ZNFPs(3)** | 40.362 | 0.0096 | 2.590 | 0.6733 | 0.00395 | 42.1941 | 0.9992 |
| **ZNFPs(4)** | 46.586 | 0.0091 | 2.565 | 0.7085 | 0.00480 | 47.8469 | 0.9999 |

- Even though the intraparticle diffusion occurs but it is not the main limiting step during adsorption process

## References


[1] Sharma, R., P. Thakur, M. Kumar, N. Thakur, N. Negi, P. Sharma & V. Sharma (2016) " Improvement in magnetic behaviour of cobalt doped magnesium zinc nano-ferrites via co-precipitation route". Journal of Alloys and Compounds, 569-581. DOI: 10.1016/j.jallcom.2016.05.200

[2] Tartaj, P., M. del Puerto Morales, S. Veintemillas-Verdaguer, T. González-Carreño & C. J. Serna (2003) The preparation of magnetic nanoparticles for applications in biomedicine. Journal of physics D: Applied physics, 36, R182. DOI: 10.1088/0022-3727/36/13/202

[3] Samavati, A. & A. Ismail (2017) Antibacterial properties of copper-substituted cobalt ferrite nanoparticles synthesized by co-precipitation method. Particuology, 30, 158-163.
DOI: 10.1016/j.partic.2016.06.003

[4] Tan, Y. F., P. Chandrasekharan, D. Maity, C. X. Yong, K.-H. Chuang, Y. Zhao, S. Wang, J. Ding & S.-S. Feng (2011) Multimodal tumor imaging by iron oxides and quantum dots formulated in poly(lactic acid)–D– alpha – tocopheryl polyethylene glycol 1000 succinate nanoparticles. Biomaterials, 32, 2969-2978.DOI: 10.1088/1468-6996/16/2/023501

[5] Caltun, O., I. Dumitru, M. Feder, N. Lupu & H. Chiriac (2008) Substituted cobalt ferrites for 294 sensors applications. Journal of magnetism and magnetic materials, 320, e869-e873. DOI: 10.1016/j.jmmm.2008.04.067

[6] Zhang, P., H. Qin, W. Lv, H. Zhang & J. Hu (2017) Gas sensors based on ytterbium ferrites nanocrystalline powders for detecting acetone with low concentrations. Sensors and Actuators B: Chemical, 246, 9-19. DOI: 10.1016/j.snb.2017.01.096

[7] Pita, M., J. M. Abad, C. Vaz-Dominguez, C. Briones, E. Mateo-Martí, J. A. Martín-Gago, M. del Puerto Morales & V. M. Fernández (2008) Synthesis of cobalt ferrite core/metallic shell nanoparticles for the development of a specific PNA/DNA biosensor. Journal of colloid and interface science, 321, 484-492. DOI: 10.1016/j.jcis.2008.02.010

[8] Willard, M., L. Kurihara, E. Carpenter, S. Calvin & V. Harris (2004) Chemically prepared magnetic nanoparticles. International materials reviews, 49, 125-170.DOI:10.1179/095066004225021882

[9] Yang, H., C. Zhang, X. Shi, H. Hu, X. Du, Y. Fang, Y. Ma, H. Wu & S. Yang (2010) Water soluble superparamagnetic manganese ferrite nanoparticles for magnetic resonance imaging. Biomaterials, 31, 3667-3673. DOI: 10.1016/j.biomaterials.2010.01.055.

[10] Bayantong, A. R. B., Shih, Y.-J., Ong, D. C., Abarca, R. R. M., Dong, C.-D., & de Luna, M. D. G. (2021). Adsorptive removal of dye in wastewater by metal ferrite-enabled graphene oxide nanocomposites. Chemosphere, 274,129518. DOI: 10.1016/j.chemosphere.2020.1

[11] Waheed Ali Khoso, Noor Haleem, Muhammad Anwar Baig & Yousuf Jamal. (2021). Synthesis, characterization and heavy metal removal efficiency of nickel ferrite nanoparticles (NFN's). Scientific Reports volume 11, 3790 DOI: 10.1038/s41598-021-83363-1

[12] Mmelesi, Olga Kelebogile; Masunga, Ngonidzashe; Kuvarega, Alex; Nkambule, Thabo TI.; Mamba, Bhekie B.; Kefeni, Kebede K. (2020). Cobalt ferrite nanoparticles and nanocomposites:Photocatalytic, antimicrobial activity and toxicity in water treatment. Materials Science in Semiconductor Processing, (), 105523–. DOI: 10.1016/j.mssp.2020.105523

[13] Kohn, J., D. Eckart & C. F. Cook (1971) Crystallography of the hexagonal ferrites. Science, 172, 519-525. DOI: 10.1126/science.172.3983.519.

[14] Moitra, A., S. Kim, S.-G. Kim, S. Erwin, Y.-K. Hong & J. Park (2014) Defect formation energy and magnetic properties of aluminum-substituted M-type barium hexaferrite. Computational Condensed Matter, 1, 45-50. DOI: 10.1016/j.cocom.2014.11.001

[15] Dietrich, R.V.. "garnet". *Encyclopedia Britannica*, 24 Jan. 2020, https://www.britannica.com/science/garnet. Accessed 27 May 2022.

[16] Tatarchuk, T., M. Bououdina, J. J. Vijaya & L. J. Kennedy. 2016. Spinel ferrite nanoparticles: synthesis, crystal structure, properties, and perspective applications. In International Conference on Nanotechnology and Nanomaterials, 305-325. Springer.

[17] Supriya, R. P. Deepali, D. A. Sandeep, B. S. Prashant, B. K. Santosh, D. M. Kamalakar, M. J. (2020) Preparation and characterisations of magnetic nanofluid of zinc ferrite for hyperthermia. Nanomaterials and Energy, 9 (1) 8-13.DOI:10.1680/jnaen.19.00006

[18] Akhtar, M. N., A. B. Sulong, M. A. Khan, M. Ahmad, G. Murtaza, M. Raza, R. Raza, M. Saleem & M. Kashif (2016) Structural and magnetic properties of yttrium iron garnet

(YIG) and yttrium aluminum iron garnet (YAIG) nanoferrites prepared by microemulsion method. Journal of Magnetism and Magnetic Materials, 401, 425-431. DOI: 10.1016/j.jmmm.2015.10.060

[19] Tatarchuk, T., M. Bououdina, J. J. Vijaya & L. J. Kennedy. 2016. Spinel ferrite nanoparticles: synthesis, crystal structure, properties, and perspective applications. In International Conference on Nanotechnology and Nanomaterials, 305-325. Springer.

[20] Sivakumar, M., T. Takami, H. Ikuta, A. Towata, K. Yasui, T. Tuziuti, T. Kozuka, D. Bhattacharya & Y. Iida (2006) Fabrication of zinc ferrite nanocrystals by sonochemical emulsification and evaporation: observation of magnetization and its relaxation at low temperature. The Journal of Physical Chemistry B, 110, 15234-15243. DOI: 10.1021/jp055024c

[21] Wan, J., X. Jiang, H. Li & K. Chen (2012) Facile synthesis of zinc ferrite nanoparticles as non-lanthanide T 1 MRI contrast agents. Journal of Materials Chemistry, 22, 13500-13505. DOI: 10.1039/C2JM30684K

[22] Moser, A., K. Takano, D. T. Margulies, M. Albrecht, Y. Sonobe, Y. Ikeda, S. Sun & E. E. Fullerton (2002) Magnetic recording: advancing into the future. Journal of Physics D: Applied Physics, 35, R157. DOI:10.1088/0022-3727/35/19/201

[23] Che, R. C., L. M. Peng, X. F. Duan, Q. Chen & X. Liang (2004) Microwave absorption enhancement and complex permittivity and permeability of Fe encapsulated within carbon nanotubes. Advanced Materials, 16, 401-405. DOI:10.1002/adma.200306460

[24] Yang, X., H. Hong, J. J. Grailer, I. J. Rowland, A. Javadi, S. A. Hurley, Y. Xiao, Y. Yang, Y. Zhang & R. J. Nickles (2011) cRGD-functionalized, DOX-conjugated, and 64Cu labelled super-paramagnetic iron oxide nanoparticles for targeted anticancer drug delivery and PET/MR imaging. Biomaterials, 32, 4151-4160. DOI: 10.1016/j.biomaterials.2011.02.006

[25] Sangita, N.P. Pratik, A.N. Arvind, V.N. Shankar, R.T. Arun, V.B. (2022) Preparation techniques for zinc ferrites and their applications: A review, Materials today proceeding 60 (3) 2194-2208

[26] Jesus, C., E. Mendonça, L. Silva, W. Folly, C. Meneses& J. Duque (2014) Weak ferromagnetic component on the bulk $ZnFe_2O_4$ compound. Journal of Magnetism and Magnetic Materials, 350, 47-49. DOI: 10.1016/j.jmmm.2013.09.025

[27] Liu, H., Y. Guo, Y. Zhang, F. Wu, Y. Liu & D. Zhang (2013) Synthesis and properties of ZnFe2O4 replica with biological hierarchical structure. Materials Science and Engineering: B, 178, 1057-1061. DOI: 10.1016/j.mseb.2013.06.012

[28] Han, L., X. Zhou, L. Wan, Y. Deng & S. Zhan (2014) Synthesis of ZnFe2O4 nanoplates by succinic acid-assisted hydrothermal route and their photocatalytic degradation of rhodamine B under visible light. Journal of Environmental Chemical Engineering, 2, 311 123-130. DOI: 10.1016/j.jece.2013.11.031

[29] Banerjee, A., S. Bid, H. Dutta, S. Chaudhuri, D. Das & S. K. Pradhan (2012) Microstructural changes and effect of variation of lattice strain on positron annihilation lifetime parameters of zinc ferrite nanocomposites prepared by high enegy ball-milling. Materials Research, 15, 1022-1028. DOI:10.1590/S1516-14392012005000135

[30] Ibrahim, A. M., M. A. El-Latif& M. M. Mahmoud (2010) Synthesis and characterization of nano-sized cobalt ferrite prepared via polyol method using conventional and microwave heating techniques. Journal of Alloys and Compounds, 506, 201-204. DOI:10.1016/j.jallcom.2010.06.177

[31] Teixeira, A. M. R. d. F., T. Ogasawara & M. C. d. S. Nóbrega (2006) Investigation of sintered cobalt-zinc ferrite synthesized by coprecipitation at different temperatures: A relation between microstructure and hysteresis curves. Materials Research, 9, 257-262. DOI:10.1590/S1516-14392006000300003

[32] Li, Q., C. Bo & W. Wang (2010) Preparation and magnetic properties of $ZnFe_2O_4$nanofibers by coprecipitation–air oxidation method. Materials Chemistry and Physics, 124, 891-322 893. DOI:10.1016/j.matchemphys.2010.07.058

[33] Qin, M., Q. Shuai, G. Wu, B. Zheng, Z. Wang & H. Wu (2017) Zinc ferrite composite material with controllable morphology and its applications. Materials Science and Engineering: B, 224, 125-138. DOI:10.1016/j.mseb.2017.07.016

[34] Gonzalez-Sandoval, M.P. Beesley, A.M. Miki-Yoshida, M. Fuentes-Cobas, L. Matutes-Aquino, J.A. (2004) Comparative study of the microstructural and magnetic properties ofspinel ferrites obtained by co-precipitation. Journal of Alloys and Compounds 369 190–194. DOI:10.1016/j.jallcom.2003.09.101

[35] Lee, H. Jung, J.C. Kim, H. Chung, Y. Kim, T.J. Lee, S.J. Oh, S. Kim, Y.S. Song, I.K. (2008) Effect of pH in the preparation of $ZnFe_2O_4$ for oxidative dehydrogenation of n-butene to 1,3-butadiene: correlation between

catalytic performance and surfaceacidity of ZnFe2O4.Catal. Commun. 9 1137–1142.DOI: 10.1016/j.catcom.2007.10.023

[36] Lee,H. Jung, J.C. Kim,H. Chung, Y. Kim,T.J. Lee,S.J. Oh,S. Kim, Y.S. Song, I.K. (2008) Preparation of $ZnFe_2O_4$ catalysts by a co-precipitation method using aqueous buffer solution and their catalytic activity for oxidative dehydrogenation of n-butene to 1,3-butadiene. Catal. Lett. 122 281–286.DOI:10.1007/s10562-007-9371-7

[37] Mostafa, H., A. Pala, J. Högel, M. Hlavac, E. Dietrich, M. A. Westhoff, L. Nonnenmacher, T. Burster, M. Georgieff& C. R. Wirtz (2016) Immune phenotypes predict survival in patients with glioblastomamultiforme. Journal of hematology& oncology, 9, 77 DOI: 10.1186/s13045-016-0272-3

[38] El-Serwy, W. S., N. A. Mohamed, W. S. El-Serwy, E. M. Kassem& A. A. Abd El Aty (2015) 305 Synthesis of new benzofuran derivatives and evaluation of their antimicrobial activities. Research Journal of Pharmaceutical, Biological, and Chemical Sciences, 6, 213-224. DOI: 10.1016/j.ejmech.2011.04.053

[39] Bean, C. & u. D. Livingston (1959) Superparamagnetism. Journal of Applied Physics, 30, S120-S129. DOI: 10.1063/1.2185850

[40] Ebrahimi, M., R. R. Shahraki, S. S. Ebrahimi& S. Masoudpanah (2014) Magnetic properties of zinc ferrite nanoparticles synthesized by coprecipitationDOI: 10.1007/s10948-014-2485-4

[41] Chinnasamy, C., A. Narayanasamy, N. Ponpandian, K. Chattopadhyay, H. Guerault& J.-M. Greneche (2001) Ferrimagnetic ordering in nanostructured zinc ferrite. Scriptamaterialia, 44, 1407-1410. DOI:10.1016/S1359-6462(01)00844-2

[42] Haghniaz, R. Rabbani, A. Vajhadin, F. Khan, T. Kousar, R. Khan, A. Montazerian, H. Iqbal, J. Libanori, A. Kim, H-J. Wahid, F. (2021) Anti-bacterial and wound healing-promoting effects of zinc ferrite nanoparticles. Journal ofNanobiotechnology, 19 (38 ) 19-38DOI:10.1186/s12951-021-00776-w

[43] McDermott, F., P., Walker D., R. and White, G., D. (2002): Antimicrobials: Modes action and Mechanisms of Resistance, International Journal of Toxicology, 22:135-143. DOI: 10.1080/10915810305089

[44] Kim, K., Sung, S., W., Suh, K., B., Moon, S., Choi, J., Kim, G., J. and Lee, G.,D., (2009): Antifungal activity and mode of action of silver nano-particles on Candida albicans. Biometals. 22:235-242. DOI:10.1007/s10534-008-9159-2. Epub 2008 Sep 4.

[45] Waranusantigula,P. Pokethitiyooka,P. Kruatrachuea,M. Upatham,E.S. (2003) Kinetics of basic dye (methylene blue) biosorption by giant duckweed (Spirodelapolyrrhiza) Environ. Pollut. 125: 385–392. DOI:10.1016/S0269-7491(03)00107-6

[46] Wu,K. Yu, J. Jiang, X. (2018) Multi-walled carbonnanotubes modified bypolyaniline for the removalof alizarin yellow R fromaqueous solutions. Adsorption Science & Technology 36(1–2) 198–214. DOI: 10.1177/0263617416687564

[47] AsifIqubal, Md. Sharma, R. Kamaluddin (2015) Studies on interaction of ribonucleotides with zinc ferritenanoparticles using spectroscopic and microscopic techniques. Karbala International Journal of Modern Science 1:49-59DOI:10.1016/j.kijoms.2015.06.001

[48] Ben Tahara,Lotfi.HabibOueslatia,M. (2020) Fast adsorption–desorption of Eriochrome Black T using superparamagneticNiZn ferrite nanoparticles. Desalination and Water Treatment. 196 315–328 DOI:10.5004/dwt.2020.26039

[49] Lagergren,S. Svenska,B.K. (1898) Zurtheorie der sogenannten adsorption geloesterstoffe, Vetenskapsakad. Handl. 24 1–39.

[50] Ho,Y.S. (2001)Sorption studies of acid dye by mixed sorbents, Adsorption 7: 139–147. DOI: 10.1023/A:1011652224816

[51] Ho,Y.S. McKay,G. (1999) Pseudo-second order model for sorption processes,Process. Biochem. 34: 451–465. DOI:10.1016/S0032-9592(98)00112-5

[52] Alkan, M. Demirbaş, O. Doğan, M. (2007) Adsorption kinetics and thermodynamics of an anionic dye onto sepiolite, MicroporousMesoporous Mater. 101: 388–396 DOI:10.1016/j.micromeso.2006.12.007